Supporting Information (SI):

Measurement Report: A comparison of ice-nucleating particle and cloud condensation nuclei

sources and properties during autumn at contrasting marine and terrestrial locations

5   Elise K. Wilbourn[1], Larissa Lacher[2], Carlos Guerrero[1], Hemanth S.K. Vepuri[1], Kristina Höhler[2],

Jens Nadolny[2], Ottmar Möhler[2], and Naruki Hiranuma[1,*]

[1]West Texas A&M University, Canyon, 79016, U.S.A.

[2]Karlsruhe Institute of Technology, Karlsruhe, Germany

10

*Corresponding author (nhiranuma@wtamu.edu)

TABLE OF CONTENTS

S1   Instrumentation

Many different instruments were used to take measurements at the Eastern North Atlantic (ENA) and Southern Great Plains (SGP) sites during the study period. The methods, as well as abbreviations, are described in the main text, but the exact model, manufacturer, and variables measured are listed in Table S1.

Table S1: A summary of instruments used in this study.

| Location	Instrument Description	Variables Measured	Model	Manufacturer	Main Text Section
ENA	Portable Ice Nucleation Experiment chamber	INP concentration, n_{INP}	PINE-3	Bilfinger Noell GmbH	2.3.1
	WT-CRAFT	n_{INP}	n/a	West Texas A&M University	2.3.2
	Condensation particle counter	Total aerosol concentration, n_{aer}	3772	TSI, Inc.	2.2
	Particle soot absorption photometer	Black carbon concentration, m_{BC}	PSAP	Radiance Research	2.5.2
	Cloud condensation nuclei counter	CCN concentration, n_{CCN}	CCN-100	Droplet Measurement Techniques	2.4
	Aerosol chemical speciation monitor	Chemical speciation	ACSM	Aerodyne Research, Inc.	2.5.1
	Weather Transmitter	Meteorological Conditions	WXT520	Vaisala	2.2
	Ceilometer	Cloud base height, planetary boundary layer height	CL31	Vaisala	2.6.1
SGP	Portable Ice Nucleation Experiment chamber	n_{INP}	PINE-3	Bilfinger Noell GmbH	2.3.1
	INSEKT	n_{INP}	n/a	Karlsruhe Institute of Technology	2.3.2
	Condensation particle counter	n_{aer}	3772	TSI, Inc.	2.2
	Particle soot absorption photometer	m_{BC}	PSAP	Radiance Research	2.5.2
	Cloud condensation nuclei counter	n_{CCN}	CCN-200*	Droplet Measurement Techniques	2.4
	Aerosol chemical speciation monitor	Chemical speciation	ACSM	Aerodyne Research, Inc.	2.5.1
	Weather Transmitter	Meteorological Conditions	WXT520	Vaisala	2.2
	Ceilometer	Cloud base height, planetary boundary layer height	CL31	Vaisala	2.6.1

*Only data from the scanning supersaturation column was used in this study.

S2   Inlet Loss Test

The loss test for the inlet used in ENA was conducted in Canyon, TX on July 14, 2021, when typical dry, dusty, and southwestern wind conditions around this region were observed. Figure S1A shows an experimental schematic of the test. As seen in the figure, the loss of particles due to gravitational settling and diffusion loss for the inlet used in ENA was quantified using an aerosol particle sizer, APS (TSI, model 3321), and two condensation particle counters, CPCs (TSI, model 3007; Palas model UF-200). The inlet was composed of a copper sampling inlet (3/8 inch outer diameter, 46-inch length) connected to a vertical sampling stack (aluminum, 6-inch diameter, 5.5 m height). Two 90° bends were involved in a copper tube one at an aerosol pickup port and another gentle bend prior to the suite of instruments. An air outflow estimated at the bottom of this particle stack was on average ≈ 80 LPM. Measurements were made for several minutes each at the top of the 5.5 m tall quasi-laminar stack inlet without any canopies and the bottom on the same day within an hour of each other (14:52 to 15:53 Local Time). TSI CPC measured 9250.6 ± 349.0 cm^{-3} and 8539.3 ± 88.2 cm^{-3} during the measurements at the top and bottom of the inlet, respectively (average ± standard deviation). Similarly, UF-200 CPC also measured 9127.7 ± 1417.5 cm^{-3} and 8217.4 ± 1185.6 cm^{-3} at each location, respectively, ensuring that all measurements were carried out with similar n_{aer} at least within the range of standard deviations. Figure S1B shows the APS-measured particle distribution at the top of the inlet (in ambient air, red) and the bottom of the inlet (through the sampling line, blue). The greatest particle loss was seen at sizes greater than 8 μm in aerodynamic diameter, with 50% particle loss occurring at diameters above 8 μm. Since the aerosol particle loss for the Portable Ice Nucleation Experiment chamber (PINE) itself is about 50 % for particles with an aerodynamic diameter of about 4 μm in aerodynamic diameter (Möhler et al., 2021), we conclude that inlet particle loss is negligible at sizes of interest for ice-nucleating particle (INP) measurements in this study.

Detailed information on the inlet particle loss testing results at SGP can be found in the Supplemental Information Figure ES12 and the associated section of Knopf et al. (2021). Briefly, the 5.5 m high inlet was constructed similarly to the inlet at ENA, with an aluminum quasi-laminar stack (6-inch diameter, 5.5 m height) connected to a copper sampling inlet with two 90° bent sections (3/8 inch diameter, 98-inch length). Particle size distribution was measured with an optical particle sizer (OPS, TSI model 3330) and CPC (TSI model 3007) at the top of the inlet and through

the inlet. Like the ENA inlet, loss of particles above 8 μm was observed. The loss of 20% of particles below 300 nm was attributed to diffusional loss.
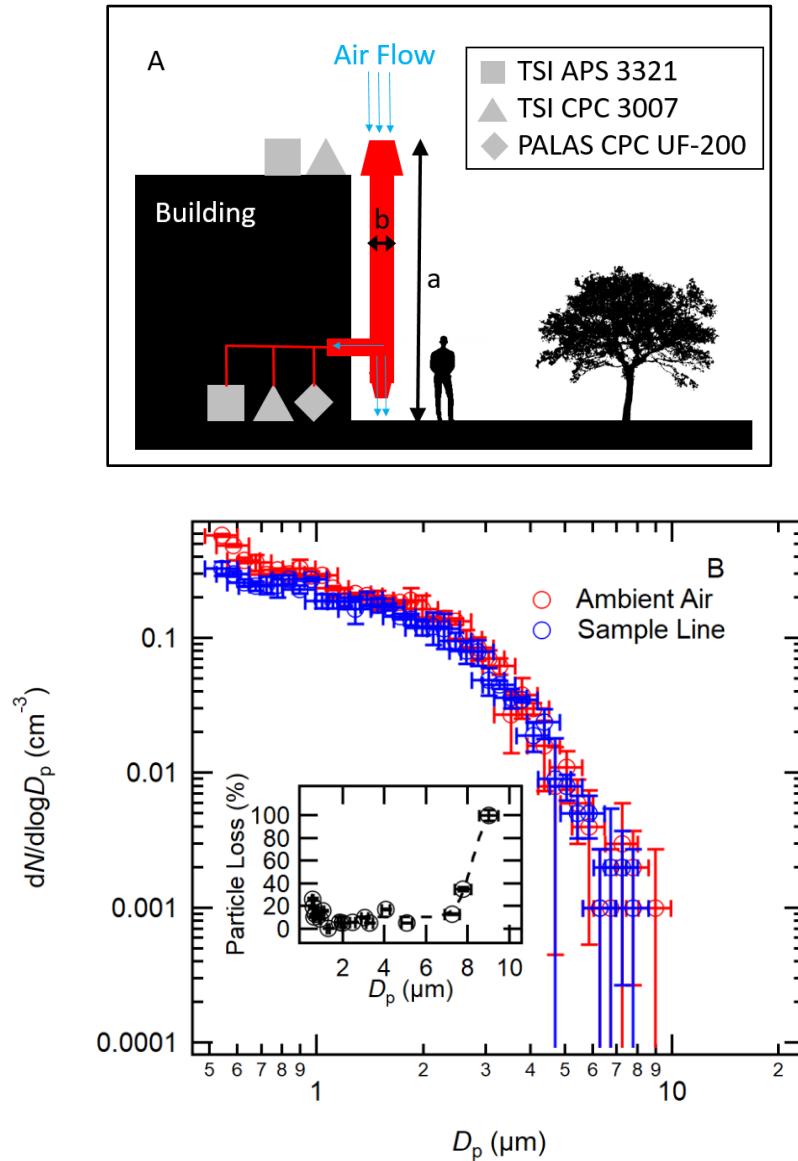
Figure S1: Panel A shows an experimental schematic of the particle loss test through the ENA stack inlet (a = 5.5 m; b = 0.1 m). Particle loss through the inlet used at ENA. Each data point is shown ± a 10.5% size uncertainty on the y-axis (Peters et al., 2006) and ± the standard deviation of three measurements on the x-axis (20-second time average for each data point). A subpanel shows calculated particle loss as a function of aerodynamic particle diameter (D_p).

S3   PINE-3 Calibration

Validations and tests of the performance of the PINE system used in this study (Bilfinger Noell GmbH, version PINE-3) were conducted after its delivery to West Texas A&M University. Specifically, we examined the freezing efficiencies of known ice nucleation active materials in immersion mode (i.e., Snomax® and illite NX) to ascertain whether previous laboratory results are reproducible with PINE-3. The immersion freezing efficiency data by means of ice nucleation active mass site density, $n_m(T)$, of Snomax® and illite NX are summarized in Wex et al. (2015, W15) and Hiranuma et al. (2015, H15), respectively.

Figure S2 A shows our experimental schematics to establish positive controls with known suspension and dry dispersed samples for PINE-3. Briefly, Snomax® suspension (0.1 wt%) was nebulized using LC SPRINT Familie nebulizer (PARI GmbH, 023G1110) for our first experiment to examine immersion freeing in the temperature range from -5 °C to -15 °C. Before aerosol-laden air reached out to buffer glassware and downstream instruments, the air was passed through a homemade 15-inch length diffusion dryer, packed with silica gels. For our second experiment, dry illite NX powder was dispersed into the downstream apparatus. To measure aerosol load in both experiments, 5-second time-resolved mass concentration measurements of particulate matter less than 10 μm in diameter (PM_{10}) were conducted using DustTrak particulate monitors (TSI Inc., Model 8520) equipped with a PM_{10} inlet. Aerosol mass concentration, measured by DustTrak, was kept at ≈ 1 μg m^3. It is noteworthy that the dew point temperature of PINE-3 was maintained at freezing temperatures in all test experiments to ensure water supersaturation conditions during each expansion run.

Figure S2 B shows the laboratory test results of heterogeneous freezing measured by PINE-3. As seen, a negligible deviation exists between our results and previous immersion freezing results. For instance, Snomax® heterogeneously froze at -7 °C as seen by other online INP instruments (Wex et al., 2015), verifying the PINE-3's applicability for high-temperature INP research. We also observed immersion freezing of illite NX at below -20 °C in PINE-3. Thus, PINE-3 was successfully calibrated to heterogeneous freezing at the examined temperature range. In addition, PINE-3 was also calibrated to the homogeneous freezing at around -34 °C (data not shown). Briefly, ammonium sulfate aerosols, nebulized using a 0.1 wt% suspension sample, froze

at ≈ -34 °C in PINE-3, which is comparable to homogeneous freezing AIDA result (Benz et al.,
110   2005; Möhler et al., 2003).
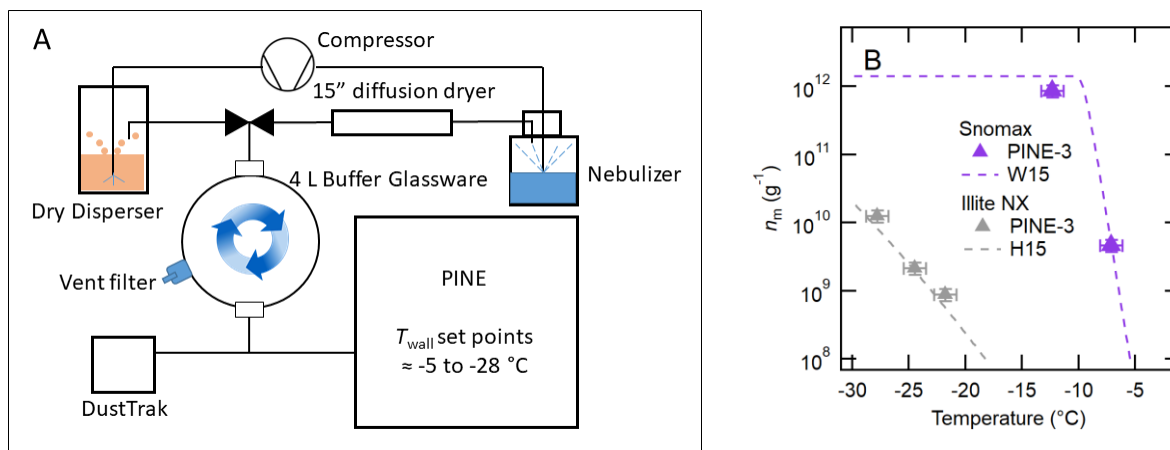
Figure S2: Experimental schematics of PINE verification experiments in panel A, and results of immersion freezing tests with Snomax® and illite NX in panel B.

S4   PINE-3 Daily Maintenance

Figure S3 shows the background test that the chamber undergoes each day to ensure that there is no source of contamination within the chamber (such as ice coating the wall and breaking off and aerosols from leaking pipelines). This process involves repeated expansions of the chamber that is filled with filtered dry air (60-second flush time) to completely replace the chamber with particle-free air. The complete emptying of the chamber can be seen in the lower panel of Figure S3, which indicates a progressive decrease in aerosol concentration during each consecutive expansion until no aerosols are present to be detected by the OPC.
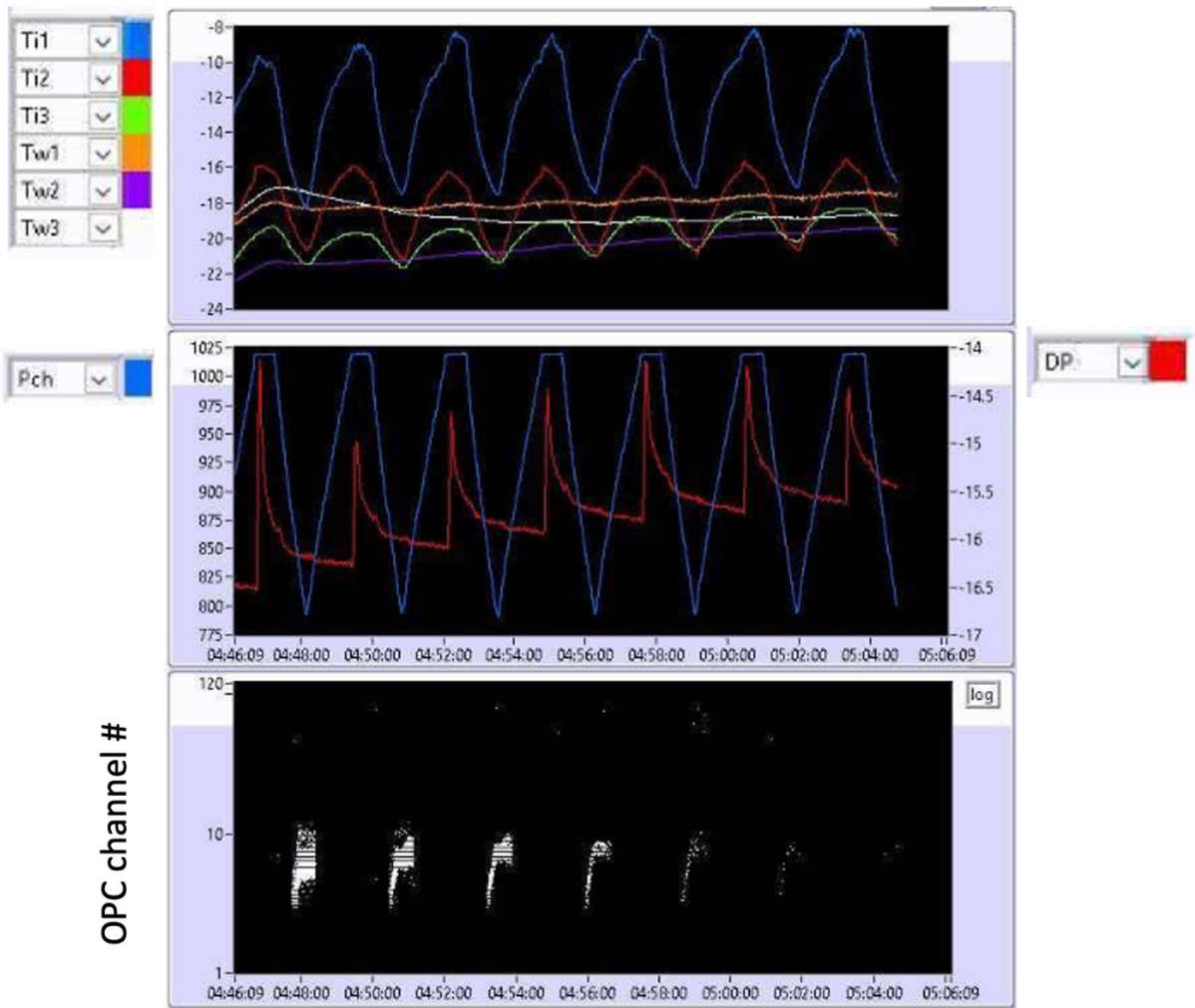
Figure S3: An example screenshot of the PINE-3 bespoke LabVIEW program monitor. Temperatures (upper panel), pressure and dew point (middle panel), and OPC measurements (lower panel) during the chamber cleaning process that is conducted each day.

7

130 **S5   PINE-3 Seasonal Maintenance**

Approximately every three months, the PINE undergoes a more in-depth de-icing process. As this process includes a complete system shutdown and reboot, on-site technical support is required (unlike the daily background test process, which is entirely remote). There are two processes that may be chosen to de-ice the chamber completely. The first process generally takes less time, as

135   the chamber is allowed to quickly warm to ≥0 °C gas temperature to defrost the ice formed on the walls in the chamber vessel while flushing filtered air through the chamber.

A longer-term procedure is occasionally needed if frost remains and the daily background procedure even after the warming/filtered-flushing procedure is unsuccessful. During this procedure, the chamber is warmed to >-5 °C in filtered flushing mode. It is then allowed to warm

140   to ambient temperature by turning off the temperature controls for >36 hours. This is generally followed by a complete system shutdown, an optical particle counter (OPC) removal from the chamber vessel, and physical removal of moisture in the PINE-3 system with assistance from an on-site technician. After rebooting the PINE-3 system, an additional 24 hours of filtered flushing typically follows at the wall temperature set at -5 °C.

145

S6   PINE-3 Leak Test

The successful operation of PINE is dependent on an airtight chamber vessel that holds pressure with little to no leaking. To ensure that our chamber was leak tight, the ability of the vessel to hold at a single pressure for several minutes was tested. Table S2 shows the leak rate at different pressures during leak tests. During these tests, the pressure inside the chamber was lowered as it would be during the expansion process. However, rather than refilling the chamber with air immediately following the pressure drop, the chamber was instead held at the lower pressure for >7 minutes with a zero set point of mass flow while the pressure was monitored, and the rate of pressure change was measured once the increase in the pressure levels off (typically it takes ≈ 2 minutes). A leak test was considered successful if the pressure increased at no more than 0.4 mb per minute. A leak test was conducted at least once per month at ENA and SGP, and no leaks were detected during either operating period. A leak test can be performed remotely.

Table S2: Pressure during PINE leak test, with low leak rate confirmed at multiple pressures.

P (mb)	Leak Rate (mb/min)
310	1.2
400	1
600	0.8
750	0.5
800	0.4
830	0.4
850	0.4
875	0.3

S7   Vibration Effect Test

During the operation of PINE-3 at ENA, there was concern over the effect of local vibrations and/or earthquakes on n_{INP}. The PINE-3 system relies on an OPC to count ice crystals, there is the possibility that any ice that might build up on the chamber wall could be shaken loose by the external vibration of the instrument. Although earthquakes are a possibility in volcanic island arcs such as the Azores, more concern was over the effect of footsteps in the vicinity of the instrument, as vibrations from footsteps could be felt passing through the trailer floor. To test this process, an onsite scientist stood in front of the instrument and jumped vigorously for 30 seconds while the chamber was undergoing an expansion to determine whether ice crystals were shaken loose. No particles that could be attributed to vibration from the vigorous jumping were observed, so it was concluded that the gentler vibrations from walking would have no effect on measured n_{INP} for PINE-3.

S8 PINE-3 Ice Threshold Determination

When PINE-3 begins an expansion, all particles are assumed to be either solid aerosol particles or activated droplets. As the expansion proceeds, the number of ice crystals increases. These ice crystals are larger than the water droplets and aerosols observed during flushing periods and are visibly above an optical size "threshold" on data from the OPC inside the PINE-3 system. This threshold is visually defined based on both the voltage of the photomultiplier within the OPC system and other environmental conditions including droplet optical particle diameter. By examining a plot of data for each operation (consisting of anywhere between one expansion and more than 100 expansions), a threshold in an optical diameter can be defined for each operation above which all particles are considered ice crystals nucleated during the expansion period. An example of the OPC data for a single operation is plotted below in Figure S4, with a dashed line indicating the threshold that was chosen for this operation. Each threshold is defined prior to any other calculations.
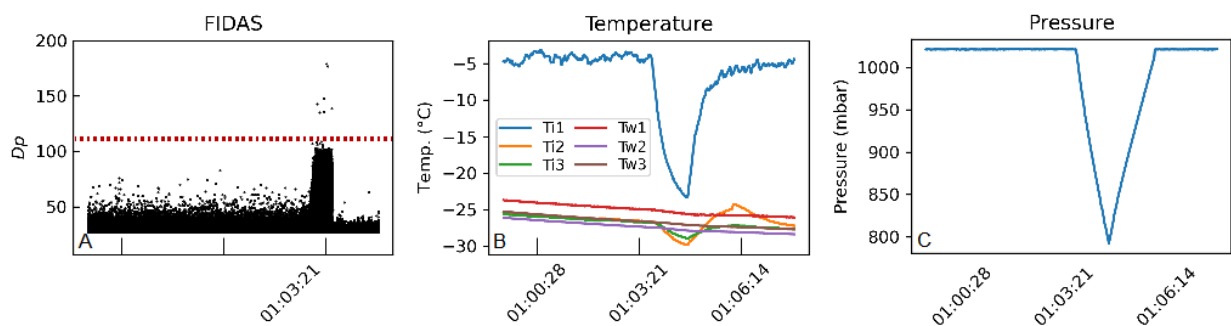
Figure S4: An example of the data used to generate a threshold level for a single operation ID. Panel A shows the data from the OPC, with the assigned threshold marked with a red dashed line. Panel B shows the wall and gas temperatures, T_w and T_i (°C). Three thermocouples located in the upper, middle, and bottom sections of the chamber vessel are denoted as 1, 2, and 3, respectively. Panel C shows the pressure inside the chamber.

S9   PINE-3 Data

The raw data generated by PINE-3 is processed into the form that is reported in this paper. The processed data are archived in publicly accessible data repository (ExINP-SGP - https://www.arm.gov/research/campaigns/sgp2019exinpsgp - ExINP-ENA; https://armweb0-stg.ornl.gov/research/campaigns/ena2020exinpena). The PINE-3 raw data includes three types of files. The detailed logbook kept during the operation of PINE is also included with raw data. The first type of raw data is the housekeeping files, which include the temperature, pressure, dew point, and valve position information. The second type of file is generated by the PINE-FIDAS and contains the particle size and concentration data that is later used to determine the threshold for each operation ID. Finally, the operation and run summary files for each operation ID contain information on the duration of each expansion and flush mode. The housekeeping files are updated when the processed data is generated, and include reference timestamps for each expansion and dew point temperatures. The timestamps included in the processed housekeeping files match those reported in the individual operation ID run summary files, which also include background n_{INP}, the ice threshold determined for the operation ID, and n_{INP}. Once all of the individual operation ID files are generated, a single data file is created by merging each of the individual files in chronological order.

S10   Statistical vs Systematic Error in PINE-3

For a discussion of the systematic error inherent in PINE-3, see Möhler et al. (2021). The temperature uncertainty estimated by Möhler et al. (2021) was ± 1 °C. To confirm this, the gas temperature sensor deviation between two thermocouples located in the bottom and upper middle section of the chamber a few centimeters off the wall was tested in PINE-3 at the SGP and ENA stations. These measurements were made during the simulated adiabatic expansions at the temperature set points of ≈ -15 °C, -20 °C, -25 °C, and -30 °C during each field campaign. At SGP, the average temperature deviation ± standard deviation at each temperature was 0.9 ± 0.5 °C, 0.9 ± 0.5 °C, 0.7 ± 0.3 °C, and 1.0 ± 0.4 °C. Likewise, at ENA, the average temperature deviation ± standard deviation at each temperature was computed as 0.4 ± 0.3 °C, 1.0 ± 0.4 °C, 0.7 ± 0.5 °C, and 0.8 ± 0.5 °C. Thus, our statistical temperature deviation at the given temperature range matches the systematic error reported by Möhler et al. (2021). The wall temperature sensor deviation was lower, ranging between less than 0.1 °C and 0.5 °C, when the wall temperature was set between -5 °C and -31 °C, while filtered air was flushed through the chamber for several hours at a time. No pattern was observed between the wall temperature set point and temperature deviation.

The statistical uncertainty in n_{INP} was estimated during the field operations at ENA at ≈ -15 °C, -20 °C, -25 °C, and -30 °C. This analysis was made based on the measurements carried out during the period of November 3, 2020 – March 1, 2021 (operation ID between 146 and 526) between four and twelve runs at each temperature. To determine the uncertainty in n_{INP} at each temperature, two types of measurements were compared and the relative error was calculated following the method described by Krishnamoorthy and Lee (2013), as well as Moore (2020). The first measurement quantifies the average amount of ice present in filtered air ($\hat{\lambda}_f$), and the second one corresponds to the average amount of ice present in a typical ambient measurement ($\hat{\lambda}_s$). These λ values were calculated using the following equation:

$$\hat{\lambda} = \frac{N}{t} \qquad\qquad\qquad [S1]$$

where N is the cumulative number of INP counted by the OPC and t is the number of expansions included in N. The ambient data at a given temperature is only considered valid if it is significantly different from the background filtered air. To determine this validity, a moment-based Z statistic (Z_m) was calculated and compared with a 90% confidence interval, using α of 0.2 and $Z_{1-\alpha/2}$ of

1.96 (valid if $Z_m > Z_{1-\alpha/2}$; otherwise, invalid). The equation used to calculate Z_m is (equation 6 given by Krishnamoorthy and Lee (2013):

$$Z_m = \frac{\hat{\lambda}_s - \hat{\lambda}_f}{\sqrt{\hat{\lambda}\left(\frac{1}{t_s} + \frac{1}{t_f}\right)}} \qquad [S2]$$

245   where

$$\hat{\lambda} = \frac{N_s + N_f}{t_s + t_f} \qquad [S3]$$

and the Poisson mean ± confidence interval (CI) can be calculated by the following equation (equation 8 given by Krishnamoorthy and Lee (2013)):

$$\hat{\lambda}_s - \hat{\lambda}_f + \frac{z^2_{1-\frac{\alpha}{2}}}{2} * \left(\frac{1}{t_s} - \frac{1}{t_f}\right) \pm z_{1-\frac{\alpha}{2}} * \sqrt{\left(\frac{\hat{\lambda}_s}{t_s} + \frac{\hat{\lambda}_f}{t_f}\right) + \frac{z^2_{1-\frac{\alpha}{2}}}{4} * \left(\frac{1}{t_s} - \frac{1}{t_f}\right)^2} \qquad [S4]$$

250

The Poisson error was calculated for the relative size of CI to Mean in % for samples taken with 300 seconds of flushing time (applicable to samples from SGP) and 600 seconds of flushing time (applicable to samples from ENA). Table S3 describes these results. As seen in the table, the estimated statistical error can exceed the systematic error in n_{INP}, ±20%, reported by Möhler et al.

255   (2021). Our error values indicate that n_{INP} measured by PINE-3 at ENA is valid for temperatures below -20 °C with a 600-second flush time or <-25 °C with a 300-second flush time.

At SGP, a similar process was used to estimate the measurement error using the data from October 15, 2019 (1400-1800 Central Time). To calculate the error, for each run, the number of aerosol particles (during the flush mode) above the determined ice crystal threshold level (during

260   the corresponding expansion mode) was defined as the background ($\hat{\lambda}_b$) in place of $\hat{\lambda}_f$. The same four equations were used to calculate the error, so:

$$\hat{\lambda} = \frac{N_s + N_b}{t_s + t_b} \qquad [S5]$$

The calculated error at ≈ -15 °C, -20 °C, and -25 °C, and -30 °C is shown in Table S4 below. While our n_{INP} measured by PINE-3 at SGP is valid for temperatures below -15 °C with a

265   300-second flush time, the estimated statistical error can exceed the systematic error in n_{INP} (±20%), especially at high freezing temperatures.

Table S3: PINE-3 Poisson mean and error in n_{INP} (L^{-1}) during times when PINE-3 was measuring the INP concentration, n_{INP}, in filtered air and unfiltered (ambient) air at ENA. The measurements of two flush periods, (A) 300 seconds and (B) 600 seconds, were independently examined. The number of expansions used for each calculation is reported as t_f or t_s for filtered and ambient air, respectively. If the measured error is statistically invalid, the mean ± confidence interval is reported as "n/a".

A. 300 Second Flush Time									
Temperature (°C)	Flush Time (s)	$\hat{\lambda}_f$	t_f	$\hat{\lambda}_s$	t_s	Mean	CI	Z_m	**Error (%)**
-15	300	0.18	4	0.06	6	-0.28	0.49	-0.57	**n/a**
-20	300	0.09	4	0.12	6	-0.13	0.44	0.17	**n/a**
-25	300	0.25	4	3.99	6	3.58	1.68	17.57	**23.34**
-30	300	3.90	4	29.52	6	25.46	4.76	95.19	**16.36**

B. 600 Second Flush Time									
Temperature (°C)	Flush Time (s)	$\hat{\lambda}_f$	t_f	$\hat{\lambda}_s$	t_s	Mean	CI	Z_m	**Error (%)**
-15	600	0.41	12	0.22	8	-0.11	0.49	-0.73	**n/a**
-20	600	0.58	12	2.14	12	1.56	0.93	5.78	**59.93**
-25	600	0.55	12	6.62	14	6.05	1.41	13.22	**23.34**
-30	600	3.46	8	26.74	8	23.28	3.81	40.15	**16.36**

Table S4: PINE-3 Poisson mean and error in n_{INP} (L^{-1}) from SGP.

Temperature (°C)	Flush Time (s)	$\hat{\lambda}_b$	t_b	$\hat{\lambda}_s$	t_s	Mean	CI	Z_m	**Error (%)**
-15	300	0.48	47	2.28	47	1.80	0.48	7.43	**26.67**
-20	300	0.53	12	6.56	12	6.03	1.51	7.85	**25.04**
-25	300	0.33	12	53.23	12	52.89	4.14	25.04	**7.83**
-30	300	0.16	8	118.29	8	118.13	7.54	30.70	**6.38**

S11   Filter-based INP Measurements

Detailed sampling periods and properties for filter samples collected at each location are summarized in Tables S5 and S6. Figures S5 and S6 show the $n_{INP}(T)$ data for individual filters from ENA and SGP, respectively. The median $n_{INP}(T)$ measured with PINE during filter sampling time is also plotted. From these plots, it becomes clear that although PINE is measuring the same aerosols, the data between online and offline data can differ by almost an order of magnitude. Briefly, at ENA the measurements made with PINE are generally higher than those made with offline measurements, while at SGP some of the measurements made with PINE are lower than those made with offline methods but approximately equal to the measurements of heat-treated samples. Further discussion of the comparison between online and offline INP measurements is available in the main manuscript Sect. 3.4.

Blank filters were also analyzed to determine whether the treated filters could be a source of error in the reported n_{INP} values. These filters were treated with peroxide using the same methods as all other filters and were randomly chosen from the prepared filters. A total of 6 blank filters was collected in the field monthly from the beginning of the campaign. For the laboratory analysis, the blank filters were suspended in 3.93 mL of HPLC-grade water (determined as the average suspension amount for filters collected at ENA) and were analyzed using WT-CRAFT with the same method described previously. The background freezing result of the blank filters is summarized in Figure S7.

Analysis of the average fraction of droplets frozen shows that there was less than one droplet frozen at temperatures above -20 °C, with only one droplet frozen on average at -20 °C. At -25 °C the blank filters averaged 6 droplets frozen. However, this is not able to explain the discrepancy between PINE and the filter data from WT-CRAFT and INSEKT, as n_{INP} from offline methods is generally lower than n_{INP} from online methods at the same temperature.

305 **Table S5: Sampling dates and times for each filter sample collected at ENA. All times given are in UTC.**

Filter ID	Start Date/Time mm/dd/yy hh:mm	End Date/Time mm/dd/yy hh:mm	Average Flow lpm	Sampling Time Min	Sampled Air Volume L	n_{INP} Detection Limit L^{-1}	Suspension Amount mL
ENA2020_04	10/5/20 14:38	10/8/20 15:08	10.9	4350	47262.8	0.001	4.93
ENA2020_09	10/8/20 15:35	10/11/20 14:08	10.8	4233	45864.6	0.001	4.78
ENA2020_11	10/11/20 14:24	10/14/20 15:30	10.7	4386	46908.3	0.001	4.89
ENA2020_14	10/14/20 15:55	10/17/20 14:30	10.7	4235	45272.2	0.001	4.72
ENA2020_18	10/17/20 15:24	10/20/20 14:24	11.1	4260	47200.8	0.001	4.92
ENA2020_20	10/20/20 14:44	10/23/20 14:17	9.6	4293	41148.4	0.001	4.29
ENA2020_22	10/23/20 14:37	10/26/20 13:50	9.4	4273	40038.0	0.001	4.17
ENA2020_23	10/26/20 14:07	10/29/20 13:24	8.8	4277	37530.7	0.001	3.91
ENA2020_26	10/29/20 13:38	11/1/20 13:30	8.7	4312	37320.4	0.001	3.89
ENA2020_28	11/1/20 13:47	11/4/20 16:03	10.8	4456	48169.4	0.001	5.02
ENA2020_30	11/4/20 16:14	11/5/20 16:33	10.8	1459	15822.9	0.001	1.65
ENA2020_31	11/10/20 9:38	11/12/20 9:05	10.9	2847	30961.1	0.001	3.23
ENA2020_34	11/12/20 9:15	11/15/20 16:22	11.4	4747	54115.8	0.001	5.64
ENA2020_36	11/15/20 16:42	11/18/20 13:24	10.0	4122	41364.3	0.001	4.31
ENA2020_40	11/18/20 13:49	11/21/20 18:05	8.6	4576	39445.1	0.001	4.11
ENA2020_41	11/21/20 18:17	11/24/20 12:16	9.5	3959	37570.9	0.001	3.92
ENA2020_43	11/24/20 12:33	11/27/20 15:25	10.3	4492	46200.2	0.001	4.82
ENA2020_44	11/27/20 15:32	11/30/20 15:50	8.7	4338	37523.7	0.001	3.91

Table S6: Sampling dates and times for filters collected at SGP. All times given are in UTC.

Filter ID	Start Date/Time	End Date/Time	Average Flow	Sampling Time	Sampled Air Volume	n_{INP} Detection Limit	Suspension Amount
#	mm/dd/yy hh:mm	mm/dd/yy hh:mm	lpm	Min	L	L^{-1}	mL
2	10/2/19 0:43	10/3/19 16:57	8.5	2414	20470.72	0.003	8.00
4	10/3/19 20:06	10/5/19 18:46	8.7	2800	24276.00	0.005	8.00
6	10/5/19 19:11	10/7/19 19:12	8.6	2881	24863.03	0.002	8.00
8	10/7/19 22:34	10/9/19 17:40	8.1	2586	21024.18	0.002	8.00
10	10/9/19 17:58	10/11/19 18:46	9.2	2928	27040.08	0.002	8.00
13	10/11/19 19:24	10/12/19 16:53	8.8	1289	11291.64	0.002	8.00
14	10/12/19 17:01	10/13/19 19:33	8.8	1592	14057.36	0.001	8.00
16	10/13/19 20:11	10/14/19 20:02	8.8	1431	12521.25	0.002	8.00
18	10/14/19 20:35	10/16/19 18:34	8.2	2759	22665.19	0.001	8.00
20	10/16/19 19:03	10/18/19 19:05	8.6	2882	24741.97	0.001	8.00
22	10/18/19 19:41	10/19/19 18:31	9.0	1370	12261.50	0.002	8.00
24	10/19/19 19:01	10/21/19 18:41	9.3	2860	26440.70	0.002	8.00
26	10/21/19 19:09	10/23/19 18:34	9.4	2845	26785.68	0.001	8.00
28	10/23/19 19:01	10/25/19 18:38	9.3	2857	26627.24	0.001	8.00
30	10/25/19 19:06	10/28/19 18:32	8.7	4286	37438.21	0.001	8.00
32	10/28/19 18:56	10/30/19 18:33	8.8	2857	25084.46	0.001	8.00
34	10/30/19 18:52	11/1/19 18:33	8.8	2861	25276.94	0.001	8.00
36	11/1/19 18:51	11/4/19 19:32	8.7	4301	37569.24	0.001	8.00
38	11/4/19 19:50	11/6/19 19:31	8.8	2861	25176.80	0.001	8.00
40	11/6/19 19:47	11/8/19 19:30	8.8	2863	25122.82	0.001	8.00
42	11/8/19 19:47	11/12/19 19:30	5.2	5743	29547.73	0.001	8.00
44	11/12/19 19:47	11/14/19 21:02	8.8	2955	26122.20	0.001	8.00
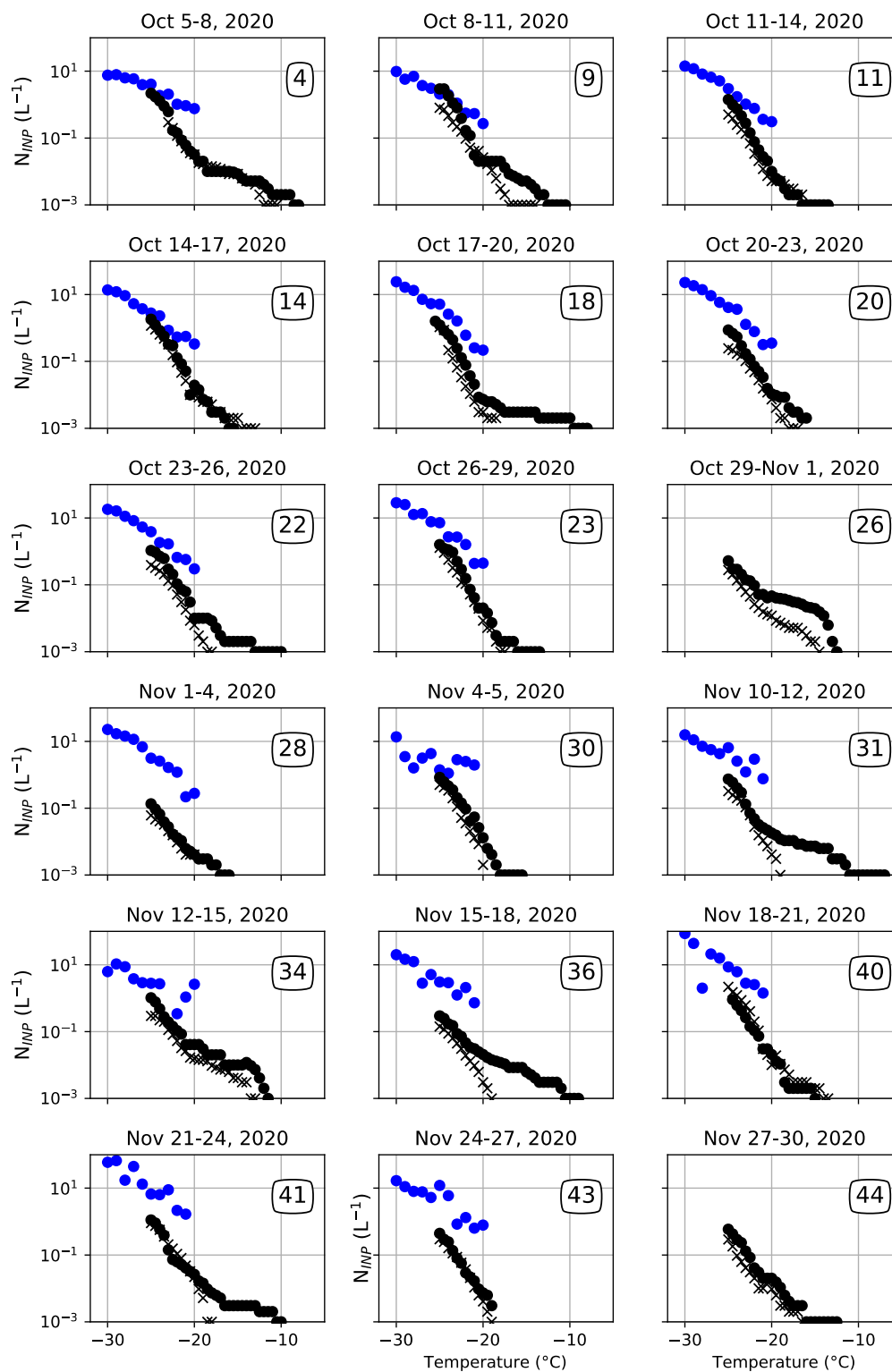
Figure S5: Ice-nucleating particle concentrations, n_{INPs}, from samples collected on filters at ENA. Untreated samples are plotted with solid dots, while heat-treated data are plotted with x's. Median data points from PINE during the same period are plotted with blue dots. The reported data are aopted from https://armweb0-stg.ornl.gov/research/campaigns/ena2020exinpena.

310
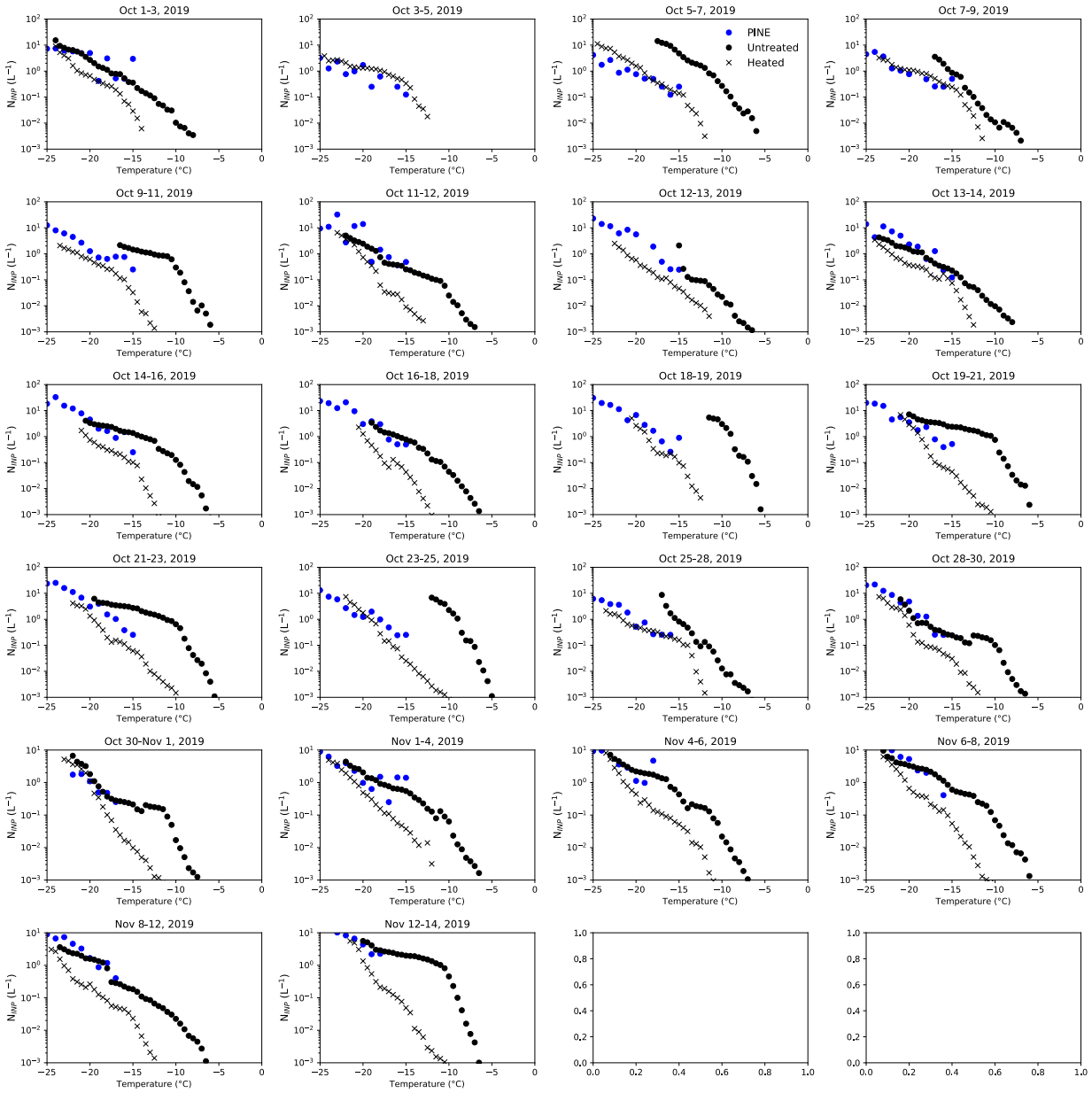
315

Figure S6: Ice-nucleating particle concentrations, n_{INPs}, from samples collected on filters at SGP. Untreated samples are plotted with solid dots, while heat-treated data are plotted with x's. Median PINE-3 data for each filter period is plotted with blue dots. The reported data are aopted from https://www.arm.gov/research/campaigns/sgp2019exinpsgp.

320
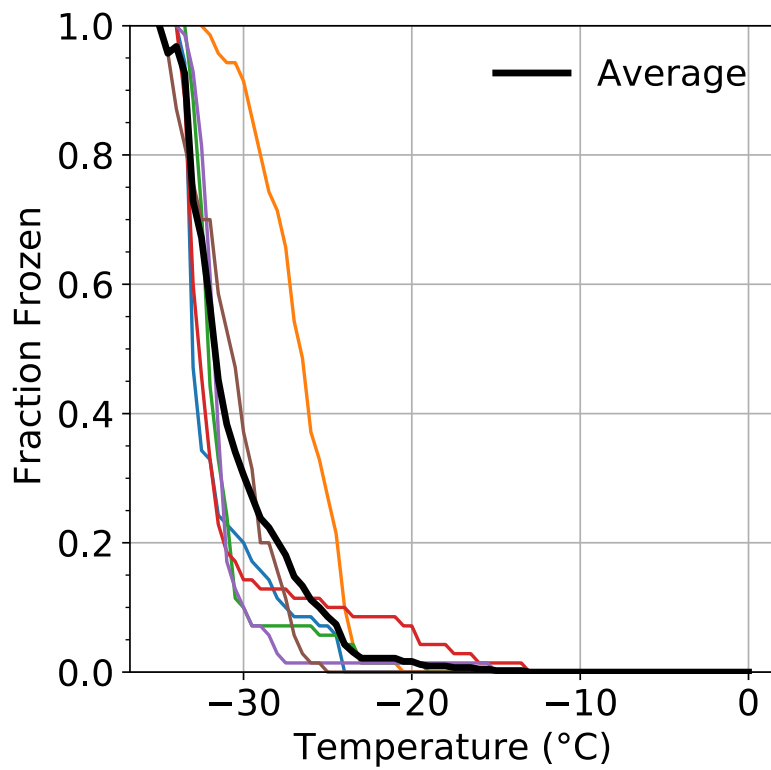
Figure S7: The fraction of droplets frozen during WT-CRAFT analysis of blank filters, with the colored lines indicating single blank filters and the heavy black line showing the average fraction frozen from all analyzed blank filters.

325

S12 Back Trajectory Origin Classification

The back trajectory origins were classified based on the oceanic or continental region the trajectory originated in either after 7 mm of rainfall occurred along the route or 240 hours prior to the origin time, whichever was less time. Ocean regions were limited to the seven major oceans (although back trajectories only originated in three of the seven seas) and large marginal ocean regions. Marginal Arctic Ocean regions were considered environmentally similar and combined into a single region consisting of the following seas: Amundsen Gulf, Baffin Bay, Barents Sea, Beaufort Sea, Chukchi Sea, Davis Strait, East Siberian Sea, Greenland Sea, Hudson Bay, Hudson Strait, Labrador Sea, Laptev Sea, and Kara Sea. The Arctic Circle category includes all North American origins with latitudes greater than 66 °N. There were no marginal Pacific Ocean seas that originated within the Arctic circle (latitude >66 °N), so all marginal Pacific Ocean seas were included within the Pacific Ocean category, including the Sea of Okhotsk, the Gulf of Alaska, and the Bering Sea. To differentiate between continents, Russia was included as a unique region from Europe. Finally, Greenland and Iceland were combined into a single category.

S13   Aerosol Characteristics

Table S7 shows the median $n_{INP}(T)$ measured with two methods addressed in this study and n_{CCN}. The given value of each measurement at each temperature is the median ± standard error, and values for both ENA and SGP are shown.

345

Table S7: An overview of aerosol properties measured at each site, with each number indicating the median value ± the standard error. Except the n_{INP} (L^{-1}) Filter data, all pther median values are based on 6-hour time averaged data.

		ENA	SGP
Time Period		Oct 1 - Nov 30, 2020	Oct 1 - Nov 15, 2019
Total Aerosols (cm^{-3})		393.25 ± 30.85	3055.00 ± 87.83
n_{INP} (L^{-1}) Filter	-10 °C	-	0.06 ± 0.17
	-15 °C	0.01 ± 0.00$_2$	0.78 ± 0.27
	-20 °C	0.02 ± 0.00$_3$	2.33 ± 0.50
	-25 °C	1.03 ± 0.18	-
n_{INP} (L^{-1}) PINE-3	-15 °C	-	0.50 ± 0.12
	-20 °C	0.36 ± 0.05	1.99 ± 0.38
	-25 °C	3.39 ± 0.48	14.40 ± 1.54
	-30 °C	15.90 ± 1.90	45.26 ± 7.86
n_{CCN} (cm^{-3})	0.1 %SS	40.58 ± 3.99	136.65 ± 7.50
	0.2 %SS	82.78 ± 8.00	402.89 ± 25.59

S14   Data Correlations

Following the same method described in Sect. 2.6.2., Spearman's rank-order correlations were used to determine the strength of relationships between collected online data from the ENA and SGP campaigns. The data sets examined here include variables measured by the instrument listed in Table S1, as well as the following particle size distribution data available through the Atmospheric Radiation Measurement (ARM) user facility data (https://www.arm.gov/data/):

- Humidified tandem differential mobility analyzer (HTDMA, Brechtel Manufacturing, Inc., Model 3002) at ENA
- APS (TSI, Inc. Model 3321) at SGP
- Scanning mobility particle sizer (SMPS, TSI, Inc. Model 3936) at SGP
- Ultra-high-sensitivity aerosol spectrometer (UHSAS, Droplet Measurement Technologies, Inc.) at SGP

In order to compare with data collected at longer time scales, all online data sets were averaged over six-hour time periods. Tables S8 and S9 summarize the results for individual variables from ENA and SGP, respectively. Further discussion of interrelations between variables is beyond the scope of this measurement report. Detailed follow-up studies are available elsewhere (e.g., Knopf et al., 2021; Raman et al., in preparation).

Table S8: The correlation coefficients calculated between variables at ENA (Spearman rank-sum correlations, ρ). All data of ρ >0.3 has a p-value <0.05 and is considered statistically significant.

	Reference time	Cloud base height	Planetary boundary layer height	$n_{INP,\,PINE}$ (-30 °C)	$n_{INP,\,PINE}$ (-25 °C)	$n_{INP,\,PINE}$ (-20 °C)	Ambient pressure	Ambient Temperature	RH	Vapor pressure	Windspeed	Wind direction	Precipitation rate (optical rain gauge)	Visibility	n_{CCN} (0.1%SS)	n_{CCN} (0.2%SS)	BC mass	CPC concentration	HTDMA(50nm)	HTDMA(100nm)	HTDMA(150nm)	HTDMA(200nm)	HTDMA(250nm)	ACSM chloride	ACSM nitrate	ACSM sulfate	ACSM total organic
Reference time	1.00	-0.02	0.17	-0.25	-0.64	-0.62	0.00	-0.66	-0.18	-0.50	0.28	0.00	0.04	-0.36	-0.64	-0.65	-0.14	-0.11	-0.51	-0.48	-0.51	-0.55	-0.58	-0.55	-0.62	-0.57	-0.59
Cloud base height	-0.02	1.00	0.16	0.02	-0.05	-0.04	-0.21	-0.11	-0.34	-0.25	-0.04	0.01	0.02	0.20	-0.03	-0.02	-0.08	0.10	0.11	0.11	0.06	0.08	0.09	-0.03	-0.07	-0.08	-0.07
PBL height	0.17	0.16	1.00	0.04	-0.10	-0.12	-0.07	-0.17	-0.24	-0.22	0.25	-0.12	0.19	-0.34	-0.08	-0.08	-0.26	0.09	-0.10	-0.11	-0.11	-0.09	-0.05	-0.01	-0.12	-0.08	-0.10
$n_{INP,\,PINE}$ (-30 °C)	-0.25	0.02	0.04	1.00	0.46	0.33	-0.12	0.22	0.08	0.17	0.02	0.11	0.08	-0.07	0.41	0.41	0.01	0.07	0.04	0.05	0.08	0.09	0.11	0.30	0.36	0.37	0.33
$n_{INP,\,PINE}$ (-25 °C)	-0.64	-0.05	-0.10	0.46	1.00	0.89	-0.09	0.48	0.20	0.39	-0.12	0.15	-0.07	0.07	0.77	0.76	-0.02	0.06	0.38	0.33	0.37	0.44	0.48	0.78	0.83	0.81	0.82
$n_{INP,\,PINE}$ (-20 °C)	-0.62	-0.04	-0.12	0.33	0.89	1.00	-0.01	0.46	0.16	0.36	-0.15	0.14	-0.07	0.14	0.81	0.80	0.02	0.06	0.41	0.37	0.39	0.46	0.49	0.81	0.80	0.82	0.80
Ambient pressure	0.00	-0.21	-0.07	-0.12	-0.09	-0.01	1.00	-0.11	-0.24	-0.22	-0.31	-0.37	-0.23	0.18	0.03	0.02	0.06	-0.22	-0.09	-0.07	-0.04	-0.06	-0.05	-0.16	-0.22	-0.18	-0.22
Ambient temp.	-0.66	-0.11	-0.17	0.22	0.48	0.46	-0.11	1.00	0.25	0.83	-0.10	-0.05	-0.17	0.24	0.50	0.49	0.42	0.32	0.42	0.40	0.42	0.46	0.41	0.34	0.41	0.42	0.41
RH	-0.18	-0.34	-0.24	0.08	0.20	0.16	-0.24	0.25	1.00	0.70	-0.15	0.05	0.11	-0.10	0.19	0.18	0.30	0.12	0.05	0.01	0.03	0.03	0.02	0.07	0.16	0.15	0.16
Vapor pressure	-0.50	-0.25	-0.22	0.17	0.39	0.36	-0.22	0.83	0.70	1.00	-0.08	-0.05	-0.03	0.05	0.39	0.38	0.44	0.28	0.27	0.24	0.24	0.28	0.23	0.22	0.31	0.31	0.30
Windspd.	0.28	-0.04	0.25	0.02	-0.12	-0.15	-0.31	-0.10	-0.15	-0.08	1.00	0.03	0.39	-0.51	-0.22	-0.21	-0.44	-0.31	-0.40	-0.38	-0.40	-0.33	-0.29	0.03	-0.04	-0.02	-0.06
Wind direction	0.00	0.01	-0.12	0.11	0.15	0.14	-0.37	-0.05	0.05	-0.05	0.03	1.00	-0.01	-0.04	0.10	0.10	-0.10	0.11	0.24	0.22	0.23	0.20	0.21	0.30	0.27	0.31	0.33
Precip. rate (optical rain gauge)	0.04	0.02	0.19	0.08	-0.07	-0.07	-0.23	-0.17	0.11	-0.03	0.39	-0.01	1.00	-0.29	-0.10	-0.09	-0.30	-0.30	-0.23	-0.27	-0.31	-0.25	-0.21	-0.01	-0.08	-0.04	-0.09
Visibil.	-0.36	0.20	-0.34	-0.07	0.07	0.14	0.18	0.24	-0.10	0.05	-0.51	-0.04	-0.29	1.00	0.19	0.20	0.39	0.04	0.33	0.32	0.34	0.29	0.23	0.03	0.04	0.06	0.05
n_{CCN} (0.1%ss)	-0.64	-0.03	-0.08	0.41	0.77	0.81	0.03	0.50	0.19	0.39	-0.22	0.10	-0.10	0.19	1.00	0.99	0.12	0.13	0.42	0.40	0.44	0.48	0.53	0.79	0.70	0.79	0.73
n_{CCN} (0.2%ss)	-0.65	-0.02	-0.08	0.41	0.76	0.80	0.02	0.49	0.18	0.38	-0.21	0.10	-0.09	0.20	0.99	1.00	0.12	0.13	0.43	0.40	0.44	0.48	0.53	0.79	0.70	0.79	0.73
BC mass	-0.14	-0.08	-0.26	0.01	-0.02	0.02	0.06	0.42	0.30	0.44	-0.44	-0.10	-0.30	0.39	0.12	0.12	1.00	0.56	0.46	0.47	0.46	0.41	0.31	-0.12	-0.03	-0.02	-0.03
CPC conc.	-0.11	0.10	0.09	0.07	0.06	0.06	-0.22	0.32	0.12	0.28	-0.31	0.11	-0.30	0.04	0.13	0.13	0.56	1.00	0.60	0.59	0.52	0.49	0.43	0.09	0.16	0.12	0.18
HTDMA (50nm)	-0.51	0.11	-0.10	0.04	0.38	0.41	-0.09	0.42	0.05	0.27	-0.40	0.24	-0.23	0.33	0.42	0.43	0.46	0.60	1.00	0.94	0.92	0.91	0.87	0.45	0.49	0.46	0.52
htdma (100nm)	-0.48	0.11	-0.11	0.05	0.33	0.37	-0.07	0.40	0.01	0.24	-0.38	0.22	-0.27	0.32	0.40	0.40	0.47	0.59	0.94	1.00	0.94	0.93	0.88	0.42	0.44	0.43	0.47
htdma (150nm)	-0.51	0.06	-0.11	0.08	0.37	0.39	-0.04	0.42	0.03	0.24	-0.40	0.23	-0.31	0.34	0.44	0.44	0.46	0.52	0.92	0.94	1.00	0.96	0.92	0.45	0.49	0.49	0.52
htdma (200nm)	-0.55	0.08	-0.09	0.09	0.44	0.46	-0.06	0.46	0.03	0.28	-0.33	0.20	-0.25	0.29	0.48	0.48	0.41	0.49	0.91	0.93	0.96	1.00	0.96	0.51	0.54	0.53	0.55
htdma (250nm)	-0.58	0.09	-0.05	0.11	0.48	0.49	-0.05	0.41	0.02	0.23	-0.29	0.21	-0.21	0.23	0.53	0.53	0.31	0.43	0.87	0.88	0.92	0.96	1.00	0.58	0.59	0.58	0.60
ACSM chloride	-0.55	-0.03	-0.01	0.30	0.78	0.81	-0.16	0.34	0.07	0.22	0.03	0.30	-0.01	0.03	0.79	0.79	-0.12	0.09	0.45	0.42	0.45	0.51	0.58	1.00	0.89	0.95	0.92
ACSM nitrate	-0.62	-0.07	-0.12	0.36	0.83	0.80	-0.22	0.41	0.16	0.31	-0.04	0.27	-0.08	0.04	0.70	0.70	-0.03	0.16	0.49	0.44	0.49	0.54	0.59	0.89	1.00	0.91	0.96
ACSM sulfate	-0.57	-0.08	-0.08	0.37	0.81	0.82	-0.18	0.42	0.15	0.31	-0.02	0.31	-0.04	0.06	0.79	0.79	-0.02	0.12	0.46	0.43	0.49	0.53	0.58	0.95	0.91	1.00	0.93
ACSM total organic	-0.59	-0.07	-0.10	0.33	0.82	0.80	-0.22	0.41	0.16	0.30	-0.06	0.33	-0.09	0.05	0.73	0.73	-0.03	0.18	0.52	0.47	0.52	0.55	0.60	0.92	0.96	0.93	1.00

Table S9: The correlation coefficients calculated between variables at SGP (Spearman rank-sum correlations, ρ). All data of ρ >0.3 has a p-value <0.05 and is considered statistically significant.

	Reference time	n_{CCN}(0.1%SS)	n_{CCN}(0.2%SS)	Cloud base height	CPC concentration	Ambient pressure	Ambient temperature	RH	Vapor pressure	Windspeed	Wind direction	Precipitation (tipping bucket rain gauge)	BC mass	ACSM chloride	ACSM nitrate	ACSM sulfate	ACSM total organic	APS number conc.	SMPS number conc.	UHSAS number conc.	UHSAS surface area conc.	UHSAS volume conc.	Planetary boundary layer height	$n_{INP,PINE}$(-30 °C)	$n_{INP,PINE}$(-25 °C)	$n_{INP,PINE}$(-20 °C)	$n_{INP,PINE}$(-15 °C)
Reference time	1.00	0.14	-0.02	-0.02	0.09	0.43	-0.62	-0.22	-0.67	-0.20	0.01	-0.19	-0.25	-0.31	0.14	-0.11	-0.13	0.03	0.20	-0.08	-0.02	0.02	-0.02	-0.29	-0.15	-0.61	-0.59
n_{CCN}(0.1%SS)	0.14	1.00	0.71	-0.20	-0.20	-0.15	0.12	0.21	0.22	0.25	-0.13	0.12	0.16	-0.06	0.39	0.54	0.42	0.64	-0.29	0.28	0.55	0.66	-0.20	-0.01	0.09	-0.21	-0.20
n_{CCN}(0.2%SS)	-0.02	0.71	1.00	0.06	0.15	-0.48	0.41	0.05	0.44	0.18	-0.07	0.04	0.18	0.00	0.22	0.35	0.77	0.60	-0.17	0.74	0.83	0.81	0.06	0.10	0.03	0.04	0.03
Cloud base height	-0.02	-0.20	0.06	1.00	0.46	-0.27	0.17	-0.40	-0.05	-0.06	0.30	-0.34	-0.14	0.05	-0.28	-0.30	0.07	-0.18	0.40	0.23	0.06	-0.03	1.00	0.27	0.08	0.35	0.30
CPC concentration	0.09	-0.20	0.15	0.46	1.00	-0.11	0.15	-0.37	-0.03	-0.26	0.15	-0.22	-0.11	-0.02	-0.09	-0.31	0.28	-0.08	0.82	0.49	0.21	0.06	0.46	-0.04	-0.23	0.11	0.12
Ambient pressure	0.43	-0.15	-0.48	-0.27	-0.11	1.00	-0.66	0.02	-0.60	-0.33	-0.10	0.00	-0.21	0.00	0.06	-0.15	-0.57	-0.34	0.17	-0.53	-0.52	-0.46	-0.27	-0.39	-0.16	-0.42	-0.42
Ambient temperature	-0.62	0.12	0.41	0.17	0.15	-0.66	1.00	-0.09	0.82	0.23	0.01	0.14	0.23	0.16	-0.21	0.26	0.51	0.23	-0.02	-0.42	0.38	0.31	0.17	0.30	0.11	0.56	0.57
RH	-0.22	0.21	0.05	-0.40	-0.37	0.02	-0.09	1.00	0.42	-0.01	-0.27	0.46	0.35	0.12	0.51	0.45	0.18	0.25	-0.51	-0.02	0.15	0.23	-0.40	0.02	0.03	-0.09	-0.08
Vapor pressure	-0.67	0.22	0.44	-0.05	-0.03	-0.60	0.82	0.42	1.00	0.17	-0.19	0.34	0.41	0.21	0.07	0.45	0.59	0.33	-0.27	0.41	0.45	0.43	-0.05	0.32	0.07	0.47	0.47
Windspeed	-0.20	0.25	0.18	-0.06	-0.26	-0.33	0.23	-0.01	0.17	1.00	-0.01	0.13	0.10	0.10	0.03	0.24	0.12	0.17	-0.35	0.01	0.14	0.17	-0.06	0.21	0.33	0.21	0.24
Wind direction	0.01	-0.13	-0.07	0.30	0.15	-0.10	0.01	-0.27	-0.19	-0.01	1.00	-0.24	-0.16	0.06	-0.16	-0.25	-0.01	-0.15	0.20	0.04	-0.04	-0.09	0.30	0.07	0.07	0.09	0.11
Precipitation (tipping bucket rain gauge)	-0.19	0.12	0.04	-0.34	-0.22	0.00	0.14	0.46	0.34	0.13	-0.24	1.00	0.26	0.16	0.20	0.36	0.12	0.09	-0.29	-0.04	0.04	0.07	-0.34	0.11	0.08	0.11	0.12
BC mass	-0.25	0.16	0.18	-0.14	-0.11	-0.21	0.23	0.35	0.41	0.10	-0.16	0.26	1.00	0.17	0.27	0.39	0.31	0.22	-0.28	0.24	0.34	0.37	-0.14	0.23	0.18	0.34	0.32
ACSM chloride	-0.31	-0.06	0.00	0.05	-0.02	0.00	0.16	0.12	0.21	0.10	0.06	0.16	0.17	1.00	-0.01	0.13	0.10	0.02	-0.06	0.04	0.04	0.03	0.05	-0.01	0.14	0.25	0.26
ACSM nitrate	0.14	0.39	0.22	-0.28	-0.09	0.06	-0.21	0.51	0.07	0.03	-0.16	0.20	0.27	-0.01	1.00	0.41	0.32	0.35	-0.24	0.23	0.36	0.42	-0.28	-0.07	0.15	-0.27	-0.30
ACSM sulfate	-0.11	0.54	0.35	-0.30	-0.31	-0.15	0.26	0.45	0.45	0.24	-0.25	0.36	0.39	0.13	0.41	1.00	0.38	0.53	-0.40	0.14	0.39	0.51	-0.30	0.10	0.09	0.12	0.14
ACSM total organic	-0.13	0.42	0.77	0.07	0.28	-0.57	0.51	0.18	0.59	0.12	-0.01	0.12	0.31	0.10	0.32	0.38	1.00	0.59	-0.12	0.86	0.88	0.81	0.07	0.18	-0.02	0.22	0.23
APS number conc.	0.03	0.64	0.60	-0.18	-0.08	-0.34	0.23	0.25	0.33	0.17	-0.15	0.09	0.22	0.02	0.35	0.53	0.59	1.00	-0.29	0.43	0.68	0.77	-0.18	-0.06	-0.03	-0.02	0.00
SMPS number conc.	0.20	-0.29	-0.17	0.40	0.82	0.17	-0.02	-0.51	-0.27	-0.35	0.20	-0.29	-0.28	-0.06	-0.24	-0.40	-0.12	-0.29	1.00	0.06	-0.19	-0.29	0.40	-0.06	-0.20	0.00	0.00
UHSAS number conc.	-0.08	0.28	0.74	0.23	0.49	-0.53	0.42	-0.02	0.41	0.01	0.04	-0.04	0.24	0.04	0.23	0.14	0.86	0.43	0.06	1.00	0.89	0.76	0.23	0.08	-0.11	-0.18	0.17
UHSAS surface area conc.	-0.02	0.55	0.83	0.06	0.21	-0.52	0.38	0.15	0.45	0.14	-0.04	0.04	0.34	0.04	0.36	0.39	0.88	0.68	-0.19	0.89	1.00	0.97	0.06	0.07	-0.02	0.10	0.10
UHSAS volume conc.	0.02	0.66	0.81	-0.03	0.06	-0.46	0.31	0.23	0.43	0.17	-0.09	0.07	0.37	0.03	0.42	0.51	0.81	0.77	-0.29	0.76	0.97	1.00	-0.03	0.06	0.02	0.04	0.05
Planetary boundary layer height	-0.02	-0.20	0.06	1.00	0.46	-0.27	0.17	-0.40	-0.05	-0.06	0.30	-0.34	-0.14	0.05	-0.28	-0.30	0.07	-0.18	0.40	0.23	0.06	-0.03	1.00	0.27	0.08	0.35	0.30
$n_{INP,PINE}$(-30 °C)	-0.29	-0.01	0.10	0.27	-0.04	-0.39	0.30	0.02	0.32	0.21	0.07	0.11	0.23	-0.01	-0.07	0.10	0.18	-0.06	-0.06	0.08	0.07	0.06	0.27	1.00	0.21	0.47	0.45
$n_{INP,PINE}$(-25 °C)	-0.15	0.09	0.03	0.08	-0.23	-0.16	0.11	0.03	0.07	0.33	0.07	0.08	0.18	0.14	0.15	0.09	-0.02	-0.03	-0.20	-0.11	-0.02	0.02	0.08	0.21	1.00	0.28	0.20
$n_{INP,PINE}$(-20 °C)	-0.61	-0.21	0.04	0.35	0.11	-0.42	0.56	-0.09	0.47	0.21	0.09	0.11	0.34	0.25	-0.27	0.12	0.22	-0.02	0.00	0.18	0.10	0.04	0.35	0.47	0.28	1.00	0.87
$n_{INP,PINE}$(-15 °C)	-0.59	-0.20	0.03	0.30	0.12	-0.42	0.57	-0.08	0.47	0.24	0.11	0.12	0.32	0.26	-0.30	0.14	0.23	0.00	0.00	0.17	0.10	0.05	0.30	0.45	0.20	0.87	1.00

REFERENCES:

375

    Benz, S., Megahed, K., Möhler, O., Saathoff, H., Wagner, R., and Schurath, U.: T-dependent rate measurements of homogeneous ice nucleation in cloud droplets using a large atmospheric simulation chamber, J. Photoch. Photobio. A, 176, 208–217, 2005.

380   Hiranuma, N., Augustin-Bauditz, S., Bingemer, H., Budke, C., Curtius, J., Danielczok, A., Diehl, K., Dreischmeier, K., Ebert, M., Frank, F., Hoffmann, N., Kandler, K., Kiselev, A., Koop, T., Leisner, T., Möhler, O., Nillius, B., Peckhaus, A., Rose, D., Weinbruch, S., Wex, H., Boose, Y., DeMott, P. J., Hader, J. D., Hill, T. C. J., Kanji, Z. A., Kulkarni, G., Levin, E. J. T., McCluskey, C. S., Murakami, M., Murray, B. J., Niedermeier, D., Petters, M. D.,

385   O'Sullivan, D., Saito, A., Schill, G. P., Tajiri, T., Tolbert, M. A., Welti, A., Whale, T. F., Wright, T. P., and Yamashita, K.: A comprehensive laboratory study on the immersion freezing behavior of illite NX particles: a comparison of 17 ice nucleation measurement techniques, Atmos. Chem. Phys., 15, 2489–2518, https://doi.org/10.5194/acp-15-2489-2015, 2015.

390   Knopf, D. A., Barry, K. R., Brubaker, T. A., Jahl, L. G., Jankowski, K. A., Li, J., Lu, Y., Monroe, L. W., Moore, K. A., Rivera-Adorno, F. A., Sauceda, K. A., Shi, Y., Tomlin, J. M., Vepuri, H. S. K., Wang, P., Lata, N. N., Levin, E. J. T., Creamean, J. M., Hill, T. C. J., China, S., Alpert, P. A., Moffet, R. C., Hiranuma, N., Sullivan, R. C., Fridlind, A. M., West, M., Riemer, N., Laskin, A., DeMott, P. J., and Liu, X.: Aerosol-Ice Formation Closure: A

395   Southern Great Plains Field Campaign, Bulletin of the American Meteorological Society, 102, E1952–E1971, 10.1175/Bams-D-20-0151.1, 2021.

    Krishnamoorthy, K. and Lee, M.: New approximate confidence intervals for the difference between two Poisson means and comparison, Journal of Statistical Computation and Simulation, 83, 2232-2243, https://doi.org/10.1080/00949655.2012.686616, 2013.

400   Moore, K. A.: Constraining marine ice nucleating particle parameterizations in atmospheric models using observations from the Southern Ocean, M.S. Thesis, Colorado State University, Ft. Collins, CO, availbale at https://mountainscholar.org/handle/10217/208435?show=full [last visisted on June 16, 2023], 2020.

405   Möhler, O., Stetzer, O., Schaefers, S., Linke, C., Schnaiter, M., Tiede, R., Saathoff, H., Krämer, M., Mangold, A., Budz, P., Zink, P., Schreiner, J., Mauersberger, K., Haag, W., Kärcher, B., and Schurath, U.: Experimental investigation of homogeneous freezing of sulphuric acid particles in the aerosol chamber AIDA,

410   Atmos. Chem. Phys., 3, 211–223, doi:10.5194/acp-3-211-2003, 2003.

    Möhler, O., Adams, M., Lacher, L., Vogel, F., Nadolny, J., Ullrich, R., Boffo, C., Pfeuffer, T., Hobl, A., Weiß, M., Vepuri, H. S. K., Hiranuma, N., and Murray, B. J.: The Portable Ice Nucleation Experiment (PINE): a new online instrument for laboratory studies and

415   automated long-term field observations of ice-nucleating particles, Atmos. Meas. Tech., 14, 1143–1166, https://doi.org/10.5194/amt-14-1143-2021, 2021.

    Peters, T. M., Ott, D., and O'Shaughnessy, P. T.: Comparison of the Grimm 1.108 and 1.109 Portable Aerosol Spectrometer to the TSI 3321 Aerodynamic Particle Sizer for dry particles, Ann. Occup. Hyg., 50, 843–850, 2006.

420   Wex, H., Augustin-Bauditz, S., Boose, Y., Budke, C., Curtius, J., Diehl, K., Dreyer, A., Frank, F.,
Hartmann, S., Hiranuma, N., Jantsch, E., Kanji, Z. A., Kiselev, A., Koop, T., Möhler, O.,
Niedermeier, D., Nillius, B., Rösch, M., Rose, D., Schmidt, C., Steinke, I., and Stratmann,
F.: Intercomparing different devices for the investigation of ice nucleating particles using
Snomax® as test substance, Atmos. Chem. Phys., 15, 1463–1485,
425   https://doi.org/10.5194/acp-15-1463-2015, 2015.